Ice Crystal Alignment: A Concept for High-Temporal-Resolution Monitoring Using Polarimetric Phased Array Radar

MARK WEBER,[a,b] DUSAN ZRNIC,[b] PENGFEI ZHANG,[b,c] AND EDWARD MANSELL[b]

[a] *Lincoln Laboratory, Massachusetts Institute of Technology, Lexington, Massachusetts*
[b] *NOAA/OAR National Severe Storms Laboratory, Norman, Oklahoma*
[c] *Cooperative Institute for Severe and High-Impact Weather Research and Operations, University of Oklahoma, Norman, Oklahoma*

(Manuscript received 14 September 2022, in final form 1 January 2024, accepted 3 January 2024)

ABSTRACT: This article describes a concept whereby future operational polarimetric phased array radars (PPAR) routinely monitor ice crystal alignment regions caused by thundercloud electric fields with volume scan updates (~12 min^{-1}) sufficient to resolve the temporal variation due to lightning and subsequent rapid electric field regeneration in nonsevere thunderstorms. Routine observations of crystal alignment regions may enhance thunderstorm nowcasting through comparison of their temporal and spatial structure with other polarimetric signatures, integration with lightning detection data, and assimilation into convection resolving numerical weather prediction models. If crystal alignment observations indicate strong electrification well in advance of the first lightning strike and likewise reliably indicate the decay of strong electric fields at the end of a storm, this capability may improve warning for lightning-sensitive activities such as airport ramp operations and space launch. Experimental observations of crystal alignment volumes in central Oklahoma severe storms and their relation to those storms' structures are presented and used to motivate discussion of possible PPAR architectures. In one case—a tornadic supercell—these observations illustrate an important limitation. Even the hypothesized 12 min^{-1} volume scan update rate would not resolve the temporal variation of the crystal alignment regions in such storms, suggesting that special, adaptive scanning methods may be appropriate for such storms. We describe how future operational phased array radars could support a crystal alignment measurement mode via parallel, time-multiplexed processing and discuss potential impacts on the radar's primary weather observation mission. We conclude by discussing research needed to better understand technical challenges and operational benefits.

KEYWORDS: Lightning; Severe storms; Supercells; Thunderstorms; Radars/radar observations; Weather radar signal processing

1. Introduction

It is well documented that the strong electric fields in thunderclouds can align ice crystals parallel to the field. Weinheimer and Few (1987) analyze the process theoretically and show that a substantial degree of alignment is expected for electric field strengths on the order of 100 kV m^{-1}, a value often observed in the electrically active regions of thunderclouds (Winn et al. 1974, 1981; Marshall and Winn 1982; Weber et al. 1982; Byrne et al. 1983). Radio waves propagating through aligned crystals are progressively depolarized owing to differences in the propagation parameters for the linear components parallel and perpendicular to the major axes of the crystals. Forward scattering from the aligned particles slows the parallel wave component and as a result, its phase advances relative to the perpendicular component. This progressive change in differential phase depolarizes the radiation unless the incident polarization is aligned with one of the principal axes of the aligned particles. A right-hand circular (RHC) wave becomes elliptically polarized with RHC and left-hand circular (LHC) components. Components of a linearly polarized (LP) wave parallel and perpendicular to the aligned particles become out of phase, likewise resulting in elliptically polarized radiation that includes a cross-polarized component relative to the incident field. As described in the paragraphs below and section 2 of this article, observational studies with dual-polarization radars demonstrate that the depolarization, and hence the crystal alignment, can be detected across the range of weather radar wavelengths using both circular- and linear-polarization bases.

Pioneering work at McGill University (Hendry and McCormick 1976; McCormick and Hendry 1979; Hendry and Antar 1982) used a dual-circular-polarization (CP) 1.8-cm wavelength radar. The radar was configured to transmit one polarization—RHC or LHC—and to simultaneously receive and process both RHC and LHC signals. Back-scattering from near-spherical hydrometeors such as raindrops converts most of the energy to the opposite polarization of that transmitted. This is the "copolar" return. The authors observed that the magnitude of the weaker "cross-polarized" return, and its cross correlation with the copolar return exhibited large values in the upper parts of thunderclouds and inferred that this was the result of progressive depolarization as the CP radiation propagated through volumes of aligned crystals. Significant decreases in the correlation between co- and cross-polar returns occurred at the time of lightning discharges as the particles became disoriented over time intervals of less than 1 s. Crystal alignment recovery times of 10–12 s are reported, presumably in association with the regeneration of strong electric fields. The authors analyzed the range-progression of the complex cross correlation

Weber's current affiliation: Retired.

Supplemental information related to this paper is available at the Journals Online website: https://doi.org/10.1175/JAMC-D-23-0028.s1.

Corresponding author: Mark Weber, mark.edward.weber@gmail.com

DOI: 10.1175/JAMC-D-23-0028.1

between the two receiver channels to quantify the differential propagation characteristics of the aligned crystal volumes, and the mean canting angle of the crystals. They observed a differential phase shift of $-2.5°$ km^{-1} in one thunderstorm and inferred canting angles (relative to the vertical) ranging from 0° to 45°. Note that Hendry and McCormick (1976) define differential phase shift in terms of differential propagation for waves polarized perpendicular and parallel to the axis of anisotropy established by ice crystal orientation, not relative to the horizontal (H) and vertical (V) polarization basis used to define the conventional differential phase variable Φ_{DP}.

Using similar methods, Krehbiel et al. (1996) present spectacular results from a dual-CP, 3-cm wavelength radar with real-time processing to detect regions of strong crystal alignment and analyze their parameters. The observations were made during the Convective and Precipitation/Electrification (CaPE) program at Kennedy Space Center, Florida, in 1991. Vertical cross sections of co- and cross-polar reflectivity, circular depolarization ratio (CDR),[1] and the magnitude and phase of the cross correlation between the two received channels are presented from a range–height-indicator (RHI) scan prior to lightning and a subsequent scan, 16 s later, during which an intracloud lightning flash occurred. In the scan prior to the lightning, regions of increased cross-polar reflectivity, high co/cross-polar signal correlation and increased CDR are observed above the melting level in association with two distinct cells within a thunderstorm. These features are absent or significantly less evident following lightning. Detailed analysis of the spatial and temporal structure of the dual-CP returns provides fascinating insights on the electrical and kinematic processes in play. The authors show that by compensating for signal-to-noise effects the progression of the depolarization with range can be estimated, which in turn allows them to map the alignment regions and the orientation of the ice crystal populations that produce them. This in turn could enable mapping the electric field structure in storms remotely. Temporal analysis in individual range gates indicate that while the inferred orientation of crystals in alignment regions returns to its predischarge value within a few seconds following lightning, the magnitude of the co/cross-polarization correlation builds back more slowly over tens of seconds. The authors infer that the recovering electric field rapidly dominates aerodynamic forces and turbulence to align smaller particles and that the fraction of aligned particles then builds over time as the electric field intensifies. The authors state that the dual-CP radar observations can reveal both the onset of strong electrification in developing storms and indicate when decaying storms are no longer likely to produce lightning.

Metcalf (1995, 1997) demonstrated that crystal alignment was readily detected at 10 cm wavelength, again using a dual-CP radar configuration. Caylor and Chandrasekar (1996) discuss how the phenomena can be detected with a LP basis and present observations of aligned crystals with the dual-wavelength CP-2 radar operating at 3 and 10 cm wavelengths. Alignment phenomena are observable in the linear depolarization ratio (LDR)[2] and specific differential phase (K_{DP})[3] polarimetric variables. A conceptual model shows that alignment-induced increases in LDR will be largest when crystals are oriented 45° relative to the vertical, and smallest for vertical and horizontal orientations. K_{DP} is positive for scatterers with their major axis oriented horizontally (e.g., oblate raindrops) and negative for ice crystals aligned vertically by the thunderstorm electric field. Their observations, again obtained in Florida during the 1991 CaPE program, show repeated buildup and dissipation of alignment signatures in the LDR and K_{DP} variables on time scales of tens of seconds, determined by the lightning flash rate. They interpret the observations using their conceptual model to infer pre- and postlightning alignment microphysics.

Crystal alignment is readily observed with the National Weather Service (NWS) operational Weather Surveillance Radar (WSR-88D), which operates in simultaneous H and V polarization mode (SHV), where both H and V signals are transmitted simultaneously and parallel H and V receiving channels are used. Ryzhkov and Zrnić (2007) analyzed the effects of aligned crystals on the propagation and scattering of SHV signals and showed that differential reflectivity (Z_{DR}) variation is complex, depending on factors such as differential phase on transmission, crystal canting angle and propagation-induced phase shifts. The result is noisy Z_{DR} "streaks" that begin at the range of the aligned crystals and continue at greater ranges for the affected radials. The authors further show that the SHV differential phase systematically decreases within vertically aligned crystal regions resulting in negative K_{DP}, consistent with the results of Caylor and Chandrasekar (1996).

Hubbert et al. (2014a,b) discuss aligned crystal measurements using the 3 cm wavelength Taiwan Experimental Atmospheric Mobile-Radar (TEAM-R) operating in SHV mode and the National Center for Atmospheric Research 10 cm wavelength S-Pol radar operating with alternating H and V transmissions (AHV). They observed regions of large magnitude K_{DP} with both positive and negative sign, which they interpreted as horizontally (or vertically) aligned smaller ice crystals coincident with larger aggregates or graupel, which resulted in near-zero Z_{DR}. Hubbert et al. (2018) discuss S-Pol AHV observations of aligned crystals during the Plains Elevated Convection at Night (PECAN) campaign in Kansas. The authors emphasize that the cross correlation between co- and cross-polarized received signals is a very sensitive indicator of aligned crystal volumes and show examples of both vertically and horizontally oriented crystal volumes.

[1] CDR is the ratio of received power in the cross- and copolarized receive channels. Typically expressed in decibel units, it is large in magnitude and negative (≤ -20 dB) when scattering is from spherical particles and the incident wave is well polarized.

[2] LDR is the inverse of the ratio of received power in the transmitted linear polarization (e.g., horizontal) to that in the orthogonal polarization (e.g., vertical). As with CDR, LDR is typically less than -20 dB when the scatterers are approximately spherical or horizontally aligned, and the incident radiation is well polarized.

[3] The K_{DP} is the rate of change with range of the phase difference between the horizontal and vertical received polarization signals. It is estimated by numerically differentiating the measured total two-way differential phase between these signals Φ_{DP}.

While these studies focused on the phenomenology of aligned crystals and their effects on radar signal propagation, there are obvious practical applications for such observations. For example, Krehbiel et al. (1996) note that "the ability to detect electrified conditions in storms by radar enables possible applications to sensitive ground operations where lightning hazards are a significant concern or to airborne operations in the vicinity of electrified storms." Hubbert et al. (2015) demonstrate this application in a case study where depolarization due to electrically aligned ice crystals is detected in a storm 11 min before the first lightning detection from the Colorado lightning mapping array. Interestingly, the depolarization could be observed at this early stage only in the co-to-cross-signal correlation and not in LDR or the presence of negative K_{DP}. Section 3a in this article discusses this practical application and others in more detail.

A significant challenge in realizing such applications is the need to monitor crystal alignment volumetrically within the storms with time resolution sufficient to resolve the temporal variation due to lightning and subsequent rapid electric field regeneration. Mazzetti and Fuelberg (2017) used data from the Earth Networks Total Lightning Network to characterize total flash rates in Florida thunderclouds for a 5-yr period (2010–14). Although rates exceeding 60 min^{-1} were observed, the vast majority of cases exhibited peak rates less than 10 min^{-1} with the upper 1.5 interquartile range less than 4 min^{-1} during the warm season. Severe thunderclouds, however, frequently exhibit rates greater than 60 min^{-1}, whether in Florida (Williams et al. 1999) or the southern Great Plains (MacGorman 1993). To avoid ambiguities between temporal and spatial variation in alignment structure, the alignment studies discussed above used volume-limited scanning ("parked beam" or successive RHIs at a single azimuth angle), which would not be feasible operationally since they would cover only a small percentage of the storm volumes of interest.

The National Oceanic and Atmospheric Administration (NOAA) is evaluating strategies for sustaining or replacing its operational WSR-88D by approximately 2040, the projected end of service life. Polarimetric phased array radar (PPAR) is one alternative under consideration, owing to the capability to scan more flexibly and efficiently using electronic beam steering (Zrnic et al. 2007; Weber et al. 2021). As described in this article, a PPAR follow-on to the WSR-88D could possibly also support a rapid-update ice crystal alignment monitoring capability that enhances NOAA's severe weather warning and forecasting mission. As we show in this article, PPAR has the potential to observe aligned crystal regions at a rate of approximately 12 volume scans min^{-1} and, in parallel, scan for the "standard" polarimetric weather variable observations at a rate of approximately 1 volume scan min^{-1}. This could potentially be accomplished using both near-instantaneous electronic repositioning of the PPAR beam(s) and digital formation of multiple, simultaneously active receive beams, which allows scan time to be reduced by a factor equal to the number of receive beams.

In the following section, we present experimental observations of aligned crystal volumes in two severe storms and discuss their relation to the storms' structures. These add to the fairly large body of previous crystal alignment studies discussed in this introduction by relating the temporal variation and spatial distribution of the aligned volumes to the severe storms' convective state and structure. In section 3, we elaborate on potential operational applications and articulate necessary capabilities for a future operational phased array radar configuration that could support both high temporal resolution and volumetric coverage for crystal alignment observations. These necessary capabilities are derived from the studies discussed in this introduction, and our crystal alignment observations in severe storms. Specific PPAR architectures that could provide the necessary capabilities are then described. In section 4, we discuss opportunities for future research using recently developed experimental PPARs and list associated research questions.

2. Ice crystal alignment observations in severe storms

Most previous polarimetric radar ice crystal alignment studies have been in nonsevere thunderstorms, although Hubbert et al. (2018) discuss such observations in a severe storm that produced large hail during the PECAN program. To obtain additional crystal alignment data in the large, frequently severe thunderstorms prevalent in the U.S. southern Great Plains, we used the NOAA/National Severe Storms Laboratory (NSSL) mobile X-band polarimetric radar (NOAA-X-POL or NOXP). Our observations complement the previous literature through discussion of crystal alignment behavior in relation to the structures and convective development states of these storms.

In section 3b, we discuss alternative polarization bases for crystal alignment observations and our preference for a dual-CP radar configuration. Since NOXP does not support the CP basis, we operated in SHV. To achieve a high temporal sampling rate, we operated NOXP in "rapid scan" RHI mode. That is, we selected an azimuth angle of interest, then continuously scanned RHIs up and down to achieve an update every 8–10 s. The RHIs scans were from 5° to 50° elevation angle with a range resolution of 0.75 km. Periodic low-elevation angle PPI surveillance scans from NOXP and data from the Oklahoma City, Oklahoma, operational WSR-88D (KTLX) were used to observe the overall structure of the storms. Unfortunately, the Oklahoma Lightning Mapping Array (OLMA) was not operating during the radar observation periods discussed in this paper. Likewise, Earth Networks intracloud lightning flash products were not available and the GOES Global Mapper (GLM) was not yet online. We were, however, able to obtain Earth Networks cloud-to-ground lightning data to compare with the radar observations.

a. *Quasi-linear convective system*

Our first case study is a quasi-linear convective system (QLCS) that propagated through the Oklahoma City metropolitan area on the evening of 26 April 2016 (UTC 27 April). NOXP operated just to the west of the National Weather Center on the University of Oklahoma campus and experienced peak wind gusts exceeding 40 m s^{-1} as the most intense portion of the QLCS passed overhead. After the system

had moved northeast of our location and begun to weaken (Fig. 1), we began systematic RHI scanning at 0228 UTC at an azimuth angle of 65° and continued until 0247 UTC by which time the QLCS had moved beyond our useful observing range.

The selected vertical scanning plane was primarily through stratiform precipitation on the northern edge of a bowing segment within the QLCS centered approximately 40 km to our southeast. Frequent cloud-to-ground (CG) lightning was observed in this area by the Earth Networks lightning detection network, with the ground strikes extending north as far as our selected scanning plane. The average CG flash rate within the QLCS bowing segment was about 4 flashes min^{-1} during the period of our RHI scanning. As discussed below, the selected RHI scan plane allowed us to observe crystal alignment behavior in the stratiform region to the north of the bowing segment, which in turn is relevant to potential operational applications discussed in section 3. It would have been valuable to simultaneously observe crystal alignment behavior in the more convective bowing segment of the QLCS. This, however, would have more than doubled the interval between successive RHIs.

The RHI scans in Fig. 2 illustrate the polarimetric signatures we used to infer the presence of aligned crystals and associated strong electric fields. Shown are the "standard" SHV polarimetric variables, that is, horizontal-polarization reflectivity Z, differential reflectivity Z_{DR}, copolar correlation coefficient ρ_{HV} and specific differential phase K_{DP}. At 0228:41 UTC a laterally extensive volume of negative K_{DP}, situated above the bright band at an altitude of 4–6 km indicates a region where ice crystals are vertically aligned by the storm's electric field. Radar reflectivity in this region is 25–30 dBZ. The large negative K_{DP} values observed (magnitude $> 1°\ \text{km}^{-1}$) indicate that a significant fraction of the crystals is aligned and that their orientation is near vertical (Caylor and Chandrasekar 1996; Ryzhkov and Zrnić 2007). Radar radials passing through this region also exhibit the Z_{DR} streaks described by Ryzhkov and Zrnić (2007), which are caused by cross coupling of the H and V signal components.

We observed lightning visually immediately after this scan. In the subsequent RHI scan (0228:51 UTC), the region of negative K_{DP} is much less evident and the extent of the Z_{DR} streak has been reduced. This indicates that the postlightning electric field in this volume no longer supports strong crystal alignment although the weaker, but still evident, Z_{DR} streak suggests that some residual alignment is present.[4] Examination of the continuous sequence of RHIs collected over the period 0228:00 to 0236:00 UTC (see animation 1 in the online supplemental material) showed repeated buildup of the crystal-alignment signatures followed by immediate dissipation after visually observed lightning. The average rate of crystal alignment signature development and dissipation inferred from these radar measurements was approximately once per minute, significantly lower than the CG rate observed by the Earth Networks system over the entire QLCS bowing segment during this period. This suggests that the electric charge in the volume we were scanning was impacted by only a subset of the flashes.

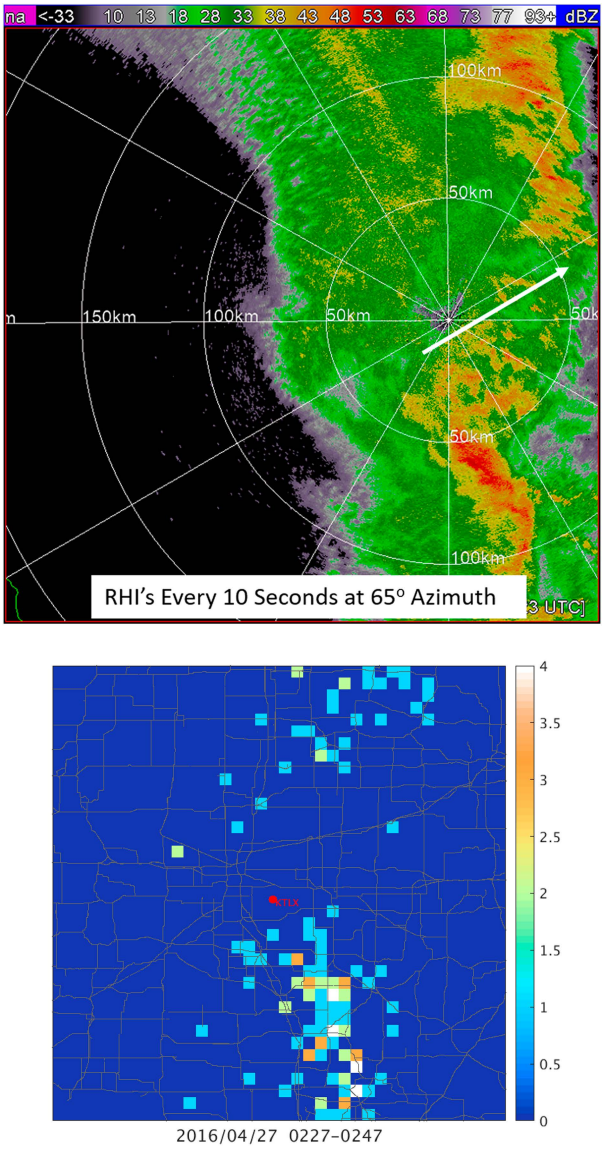

FIG. 1. (top) KTLX reflectivity PPI base scan and (bottom) Earth Networks cloud-to-ground lightning detections during the period (0228–0247 UTC 27 Apr 2016) in which we collected systematic rapid-scan RHIs with NOXP along the 65° radial as indicated by the arrow.

Figure 3 shows a KTLX synthetic reflectivity RHI at 170° azimuth. The bowing segment of the QLCS to our southeast extended above 12 km AGL. Although winds were strong and from the west at the surface, they backed

[4] As noted in section 1, Krehbiel et al. (1996) observed that initial crystal realignment occurs within a few seconds following lightning and that the magnitude of the alignment then continues to build over tens of seconds. Given the 10-s revisit intervals for our observations, it is not surprising that we continued to observe weak alignment signatures on scans immediately following lightning.

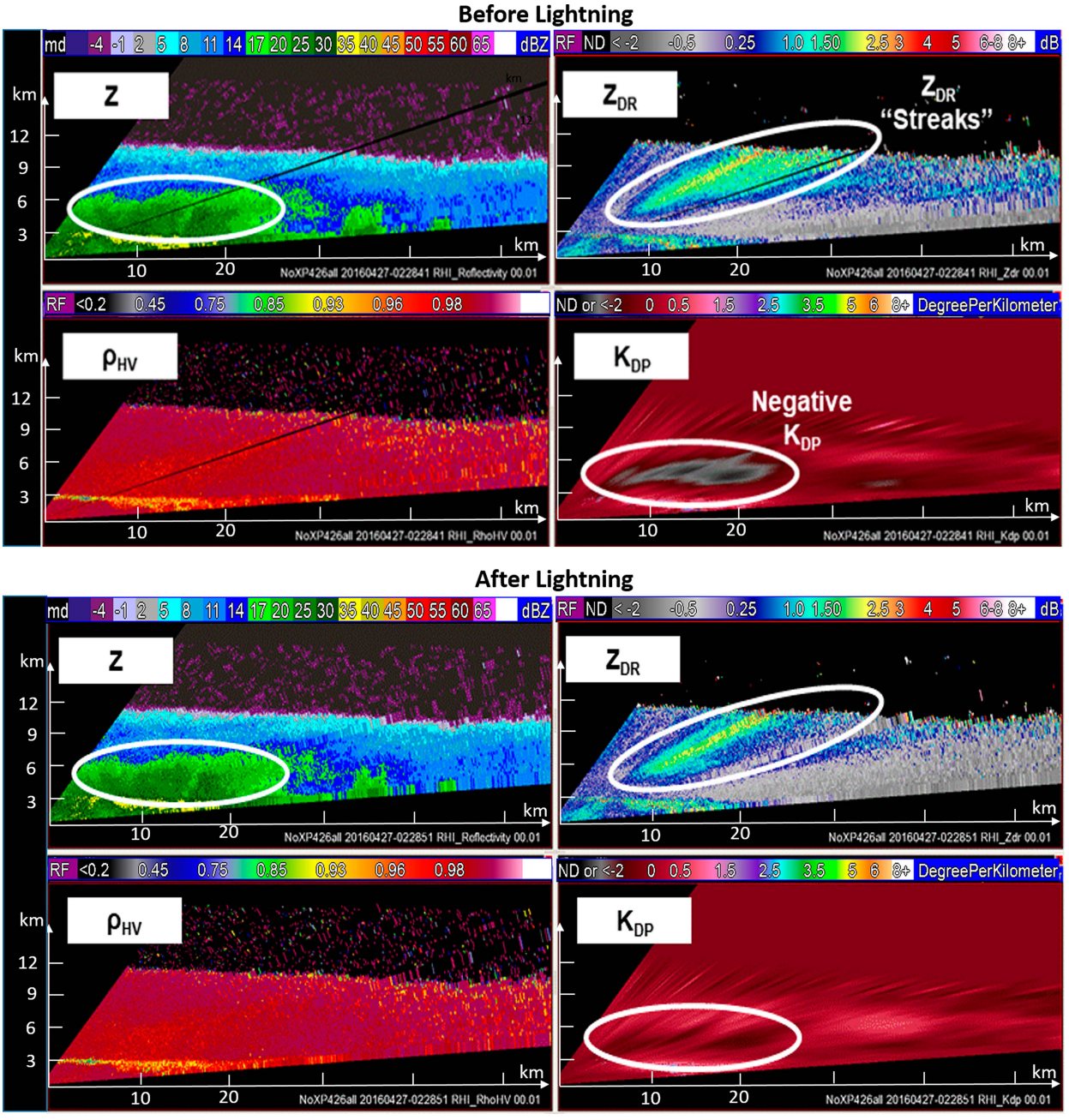

FIG. 2. NOXP RHI scans of polarimetric variables at (top) 0228:41 UTC and (bottom) 0228:51 UTC 27 Apr 2016.

quickly with altitude and were southerly above about 1 km AGL.[5] At 5 km AGL winds were almost 25 m s^{-1}, possibly resulting in the advection of charge into the stratiform region through which we scanned. Alternately, local separation of charge in the stratiform region of this storm, as discussed by Rutledge et al. (1993), may have been a more significant contributor to the observed crystal alignment volumes. As suggested by our radar observations, some of the lightning flashes tapped charge in the stratiform region north of the QLCS element and, as a result, flashes came to ground well north of the area of most active charge separation. In the absence of OLMA data, which could have provided detailed reconstructions of the individual flashes, our interpretations are necessarily speculative.

[5] The wind profile was estimated using the State of Oklahoma Mesonet station at the National Weather Center in Norman (surface wind) and inspection of the KTLX radial velocity profile variation with range (height) on midelevation scans.

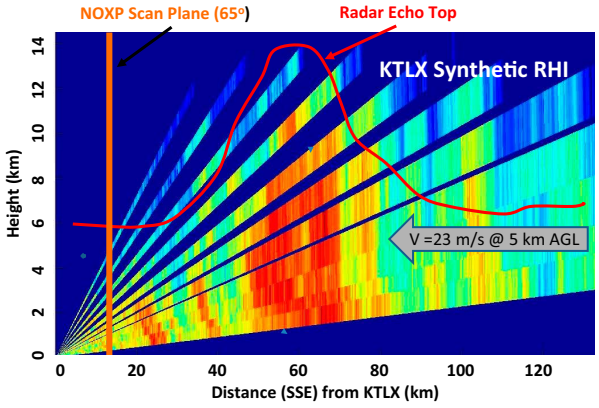

FIG. 3. Synthetic RHI from KTLX for QLCS on 27 Apr 2016.

b. *Discrete supercell*

Our second case study (Fig. 4) is a discrete supercell on 29 April 2016, whose northern section we scanned for a short period (2055–2102 UTC) as it approached the Oklahoma City metropolitan area. This storm produced an EF1 tornado in Commanche County at approximately 2040 UTC, an EF0 tornado in Caddo County at 2054 UTC and an EF1 tornado in Grady County at 2111 UTC, all communities southwest of Norman, Oklahoma. The Earth Networks CG data indicated intense CG rates during the period we were scanning (average rate 14.6 min^{-1}). Given the large intracloud (IC) to CG ratio for supercell storms (Schultz et al. 2011) it is likely that the total lightning rate in this storm was once per second or higher.

Not surprisingly then, in contrast to the previous case, our 8–10-s scanning period was not sufficient to define the temporal variation of the crystal alignment signatures. Instead, we observed a persistent volume of negative K_{DP} at altitudes of 6–12 km along with down-radial Z_{DR} streaks. These alignment signatures, illustrated in Fig. 5 and animation 2 in the online supplemental material, fluctuated considerably in size, intensity, and small-scale structure over the 8 min scanning period but there were no scans where these suddenly and fully dissipated. Bruning and MacGorman (2013) show that lightning near supercell updrafts occurs at very high rates, but with relatively small spatial extents. Since our scan revisit time (10 s) was long relative to the flash rate in this storm, we are not able to resolve the rapid buildup and dissipation of crystal alignment associated with the small pockets of charge responsible for the high-rate lightning. This contrasts with the preceding case where the spatially extensive charge region in the QLCS anvil would form and dissipate over a much longer period and produce lightning that is larger in spatial extent. It likewise contrasts with the nonsevere thunderstorm observations discussed in the introduction, where build up and dissipation of the crystal alignment signatures occurs on time scales of 10s of seconds.

The negative K_{DP} region was coincident with moderate reflectivity values (35–40 dBZ) above the highest reflectivity in the scan plan and again exhibited large magnitude negative values (magnitude $> 1°\ \text{km}^{-1}$). Smaller, less persistent regions

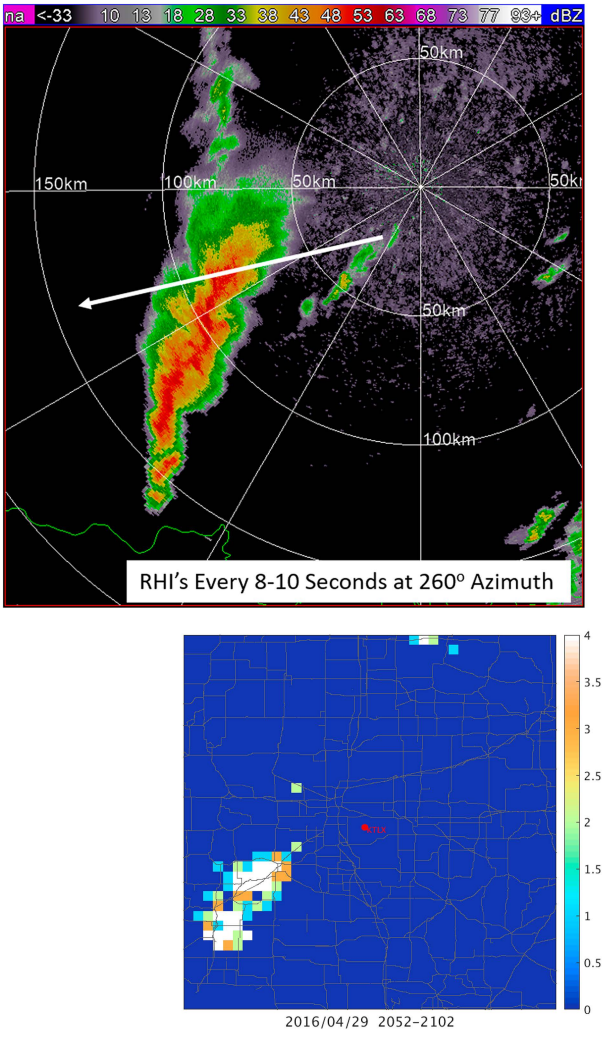

FIG. 4. As in Fig. 1, but during the period 2055–2102 UTC 29 Apr 2016 and along the 260° radial.

of negative K_{DP} were observed in lower reflectivity volumes on the western (trailing) side of the supercell.

Figure 6 shows KTLX PPI variable fields at various elevation angles. Our RHI scanning plane was north of a vertically continuous, rotational signature with an associated Z_{DR} column. This indicates a strong, organized updraft, undoubtably resulting in significant charge separation. It is possible that the upper-level flow carried charge northward through the volume we scanned and contributed to the strong electric fields inferred from the persistent K_{DP} and Z_{DR} alignment signatures (Fig. 5). As noted, the 8–10-s RHI sampling period was not sufficient to determine whether the very frequent lightning in the supercell was discharging this volume.

3. PPAR ice crystal alignment monitoring architectures

The ice crystal alignment studies discussed in section 1 and the observations described in section 2 illustrate both opportunities for improving real-time monitoring of the electrical

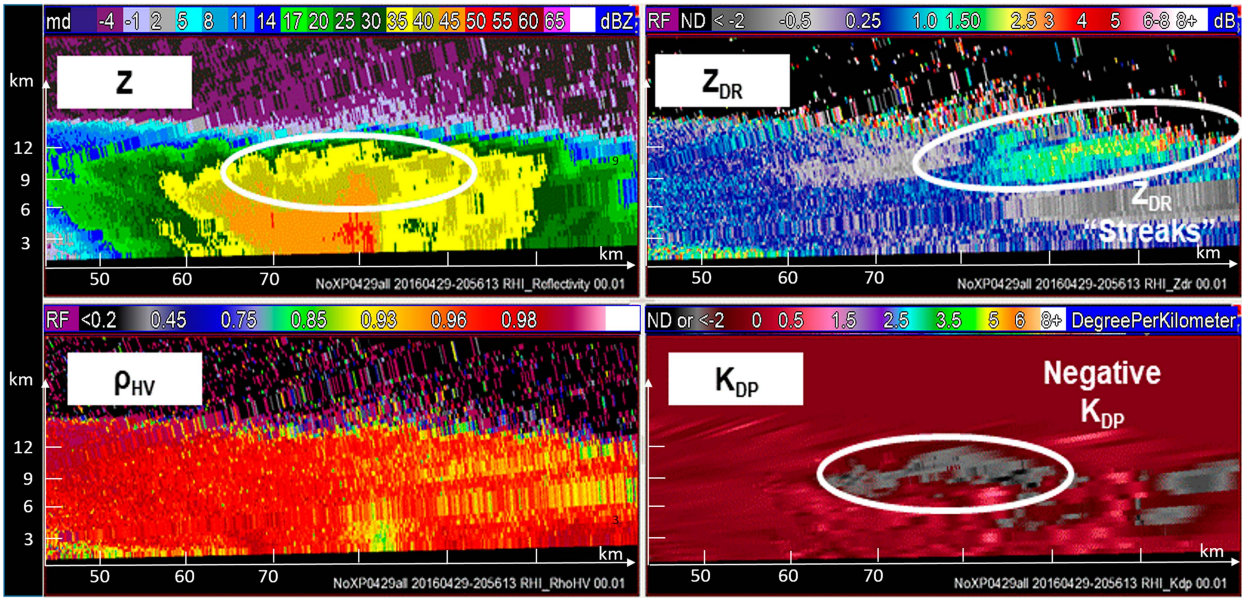

FIG. 5. NOXP RHI scan of polarimetric variables at 2056:13 UTC 29 Apr 2016.

(and indirectly the convective) state of thunderstorms and challenges associated with achieving volumetric temporal sampling sufficient to observe crystal alignment behavior during the rapid buildup and dissipation of charge volumes. The thesis of this article is that next-generation operational PPARs may be able to observe crystal alignment volumetrically with an appropriate sampling rate and that this, in turn, may enhance operational severe weather warnings. In this section, we first discuss potential operational applications of a robust crystal alignment monitoring capability, then describe PPAR architectures that could allow these to be realized.

a. Operational applications

Our observations of crystal alignment in the anvil region of a QLCS are relevant to the challenge of operational lightning warnings for ground activities near—but not directly underneath—strong, electrically active convective cells. A good example is airline ramp operations where baggage handling and refueling need to be suspended when there is a threat of ground strikes. Current decisions on ramp operation shutdowns and resumptions are based on lightning detection systems. Typically, the ramp is closed in response to a first lightning strike within a critical distance of the airport and then reopened after a wait period following the last nearby strike (Heitkemper et al. 2008; Steiner et al. 2014). Uncertainty as to the "optimal" values for the critical distance and wait-period parameters may lead to compromised safety or unnecessarily long ramp closures. If further studies, as suggested in the last section of this paper, show that the presence or absence of aligned crystal signatures in the stratiform region surrounding an active cell is a robust indicator of whether ground strikes may occur, then more effective decision support for such lightning-sensitive ground operations may be possible.

Data assimilation (DA) of radar reflectivity and radial velocity observations into numerical weather prediction models has been demonstrated to improve the short-term forecast of high-impact weather events such as severe thunderstorms (e.g., Stensrud and Gao 2010; Schenkman et al. 2011; Yussouf et al. 2016; Jones et al. 2016). Likewise, DA of total lightning observations, now available continuously in the Western Hemisphere from the GLM on GOES-R, can improve short-term forecasts of storm evolution (Fierro et al. 2019). Krehbiel et al. (1996), Caylor and Chandrasekar (1996), and Hubbert et al. (2014a,b, 2015, 2018) discuss a number of instances where the crystal alignment observations allow for detailed inferences on storm microphysical conditions. The case studies in section 2 exhibit quite different spatial structure and temporal variation for the aligned crystal volumes, reflecting the very different convective conditions in the storm volumes observed. If crystal alignment observations were available volumetrically and throughout the life cycle of thunderstorms, it would be valuable to explore appropriate techniques for assimilating the information they convey on electrical and microphysical structure, and to assess whether it improves model forecasts beyond what can be achieved using traditional radar variables and lightning detection data.

More broadly, volumetric, high-update crystal alignment observations would complement the toolkit of thunderstorm electricity based severe weather warning diagnostics. Volumetric monitoring of ice crystal alignment regions would provide unprecedented information on the electric field structure inside thunderclouds (Krehbiel et al. 1996), which in turn is driven by critical convective processes such as updraft intensity, supercooled liquid water content and mixed-phase interactions between graupel and ice crystals (Deierling et al. 2008; Schultz et al. 2015). The locations and parameters of crystal

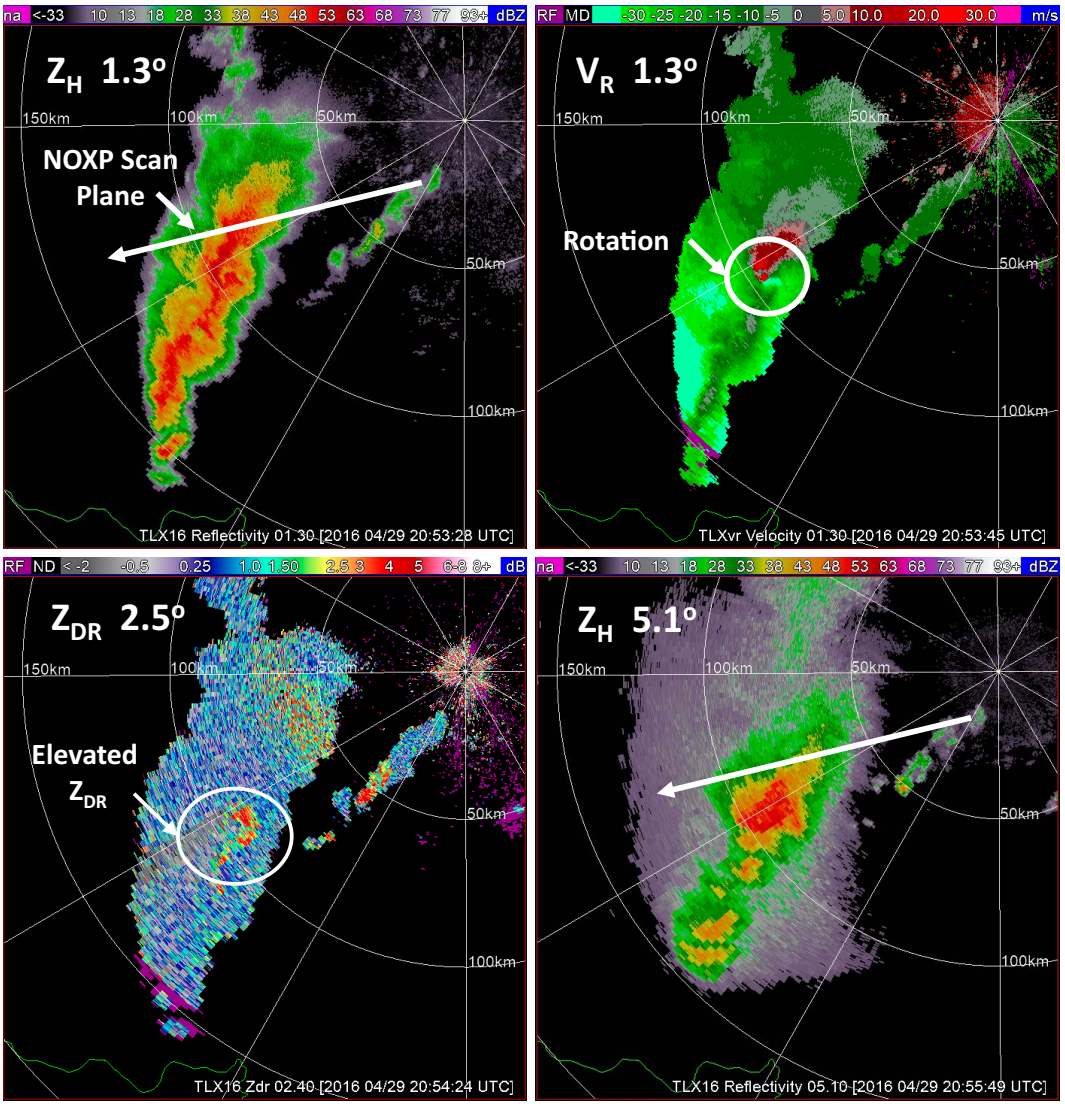

FIG. 6. KTLX WSR-88D PPI observations of the tornadic supercell on 29 Apr 2016. The elevated Z_{DR} column locates the center of the updraft.

alignment regions, when correlated with other polarimetric signatures such as differential reflectivity Z_{DR} columns, may facilitate inference of the location, vertical extent—and thereby the intensity—of thunderstorm updrafts (A. V. Ryzhkov 2016, personal communication). Rapid increases in the total lightning rate or "lightning jumps" (Williams et al. 1989; Schultz et al. 2009; Gatlin and Goodman 2010) have been shown to be associated with explosive updraft intensification in severe storms, and observed to precede large hail, tornadoes, or strong winds at the surface by many minutes. Volumetric monitoring of crystal alignment may complement lightning detection systems via spatial localization of strongly electrified volumes and/or greater sensitivity to the onset of the lightning jump phenomenon. Finally, the ability of phased array radars to examine rapid changes in the reflectivity structure of thunderstorms, in conjunction with lightning mapping array data, has been shown to provide valuable information on the potential for rapid storm intensification and decay, and associated lightning activity (Emersic et al. 2011; Yoshida et al. 2017). PPAR's ability to observe rapid variations in reflectivity (and other radar variables), coupled with robust crystal alignment observations would provide important observations for short-term forecasts of storm evolution.

b. *Notional capabilities*

As shown in the introduction and case studies, electrical alignment can be detected using dual-CP, AHV, or SHV linear polarization. Additionally, a linear polarization method often referred to as LDR mode, in which H signals are transmitted and both H and V signals are received, enables observation and measurement of LDR and correlation of the

copolar field with the cross-polarized field resulting from the aligned crystals (Melnikov et al. 2019; Hubbert et al. 2018). The SHV mode does not allow for direct measurement of the cross-correlated field component and quantitative estimation of the intensity of the alignment and the canting angle of the crystals. (Our choice of this mode for the observations in section 2 was driven by the configuration of the NOXP radar available to us.) AHV- and LDR-mode linear polarizations may have substantially weaker correlation values than CP because LP transmissions are not depolarized by particles aligned parallel or perpendicular to the direction of polarization. (Aligning the transmissions at 45° may mitigate this issue when crystals are aligned vertically or horizontally as is often the case.) For these reasons, we believe that the dual-channel CP method used by McCormick and Hendry (1979), Krehbiel et al. (1996), and Metcalf (1995, 1997) is an attractive approach since its performance is not sensitive to the canting angle of the depolarizing ice crystals. For specificity, subsequent discussion of PPAR architectures will assume that the dual-CP method is employed.

A volumetric sampling rate of 12 min^{-1} is assumed as an achievable capability that is greater than the maximum flash rate in most nonsevere thunderclouds (Mazzetti and Fuelberg 2017). In some severe storms, this sampling rate would not resolve temporal variation due to lightning, particularly on the scale of the small lightning discharges discussed previously. However as illustrated in the second case study in section 2, the overall structure of the aligned crystal volumes in a severe storm with high flash rates may be relatively stable, suggesting that the large-scale electric field structure may also be persistent over intervals significantly longer than the proposed sampling interval. Once such volumes are identified, adaptive scan patterns over limited azimuth and/or elevation angles may be initiated to increase the sampling rate.

The aligned crystal regions described in the previous section occurred in association with copolar reflectivity factors of 25–40 dBZ. Caylor and Chandrasekar (1996) state that crystal alignment regions typically coincide with reflectivity factors of 35 dBZ or less. Images presented by Krehbiel et al. (1996) show volumes of high CDR and high co/cross-polar signal correlation in association with reflectivity factors as low as 12 dBZ. Based on these observations, we propose that the crystal monitoring capability should have sensitivity sufficient to observe a 10-dBZ echo with 0-dB single-pulse signal-to-noise ratio (SNR) at a range of 100 km. This is approximately 14 dB less sensitive than the WSR-88D.[6]

Last, we will assume that coherent processing intervals (CPI) used for ice crystal alignment monitoring are 0.020 s, within the 0.016–0.022-s range used for estimation of polarimetric variables with the WSR-88D.

As described below, the ice crystal alignment monitoring would be performed in parallel with "standard" weather variable observations over full volume coverage patterns (VCP) that include the crystal alignment regions. For these observations, the PPAR would provide sensitivity, angular resolution, and CPIs (i.e., data quality) equivalent to the WSR-88D. The volume scan update rate for the standard weather variables would be approximately 1 min^{-1}.

c. *Four-face planar array*

One possible sensor configuration is based on the Multifunction Phased Array Radar (MPAR) concept (Weber et al. 2007) that was a basis for Federal Aviation Administration (FAA) and NOAA phased array radar research between 2006 and 2017 (Stailey and Hondl 2016). This concept envisioned a four-faced, highly digital PPAR with sufficient sensitivity, aperture size and beam agility to simultaneously perform the missions accomplished today by FAA air surveillance radars, Terminal Doppler Weather Radars (TDWR), and the NOAA WSR-88D. Of particular relevance to this discussion is MPAR's aircraft volume search function, illustrated in Fig. 7 and described in detail by Weber et al. (2017). An overlapped subarray antenna architecture enables clusters of digitally formed receive beams to be formed. These provide simultaneous, angle-resolved surveillance across the solid angle illuminated by a transmit beam that is purposely broadened ("spoiled") by applying a phase-taper across the aperture. The volume search pattern depicted in the table exploits the resulting large reduction in the number of transmit-pulse pointing angles to surveil a 90° (azimuth) by 17° (elevation) sector in 4.3 s. Although NOAA and FAA are no longer pursuing the MPAR concept, we will show how MPAR's aircraft surveillance channel could have supported a parallel, ice crystal alignment monitoring function without adversely affecting its primary mission. This is relevant since future FAA or military air surveillance radars may utilize four-faced array architectures similar to that described and could therefore support a dual-use crystal monitoring mode for weather warning applications. This "side car" processor would be analogous to the Airport Surveillance Radar (ASR-9) Weather Systems Processor (WSP) developed by the FAA to provide wind shear protection services at medium-density airports (Weber and Stone 1995) and would be constrained to observe only the elevation angles scanned for aircraft surveillance.

Air surveillance radars utilize circularly polarized signals to increase the aircraft signal-to-precipitation power ratio. When scattered from nearly spherical hydrometeors, the polarization sense is reversed, and this power ratio increases by 15 dB or more when the polarization corresponding to the transmitted pulse is processed. "Weather channels" on these radars process the opposite sense signals to maximize the SNR for precipitation returns.

The proposed processing to monitor ice crystal alignment exploits this circumstance as shown in Fig. 8. Each of the array's transmit–receive (TR) elements consists of parallel H and V polarization channels. For aircraft search, these are phased to transmit, say, LHC signals. Received signals in both channels are processed and combined to form both LHC and

[6] This notional capability for sensitivity relative to the WSR-88D and the following notional capabilities for CPI length and standard weather variable update rate are based on NOAA/National Weather Service Radar Functional Requirements (NWS 2015).

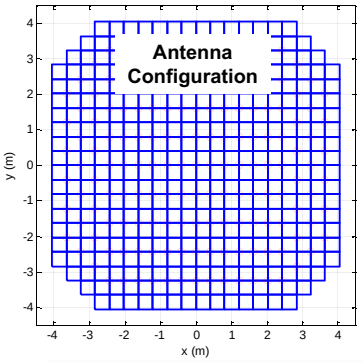

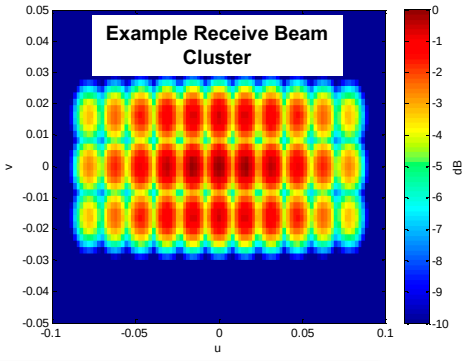

Aircraft Search Pattern

Elevation Angle (deg)	Average PRT (μs)	Rx Beam Cluster Size	Number of Tilts	Scan time per tilt (s)	Pulse Width (μs)	SNR Margin (dB)
0.5	3804	7	1	0.967	190	6.7
1.4	3804	9	1	0.752	190	4.7
2.3	3745	9	1	0.741	187	4.9
3.2	3190	11	1	0.516	159	5.2
4.1-5.0	2753	18	2	0.272	138	4.9
5.9-8.6	2130	36	4	0.105	107	5.3
9.5-12.2	1438	48	4	0.052	72	7.2
13.1-15.8	1079	48	4	0.039	54	11.0
Total Scan Time				4.3 s		

FIG. 7. Notional MPAR aircraft volume search pattern (from Weber et al. 2017). The 8-m-diameter antenna face is segmented into 159 overlapped subarrays. The subarray outputs are digitized and processed to form clusters of simultaneous receive beams, spanning a solid angle matched to a spoiled transmit beam. The volume search pattern varies the pulse repetition interval, receive beam cluster size, and (uncompressed) pulse width to meet elevation-angle-dependent unambiguous range and sensitivity goals. Individual receive beam widths are approximately 1° at broadside to the array. The angular coordinates in the beam cluster image are "u" ($\sin\Phi\cos\Theta$) and "v" ($\sin\Theta$), where Φ and Θ are the azimuth and elevation angles of the beam relative to the normal to the array. The horizontal axis u therefore represents the azimuth extent of the beams, and the vertical axis v represents their elevation extent.

RHC channels with the LHC channel providing the primary input for aircraft surveillance. For ice crystal monitoring, both signals are inputs to a pulse-pair correlator that generates the indicated polarimetric variables. This processing is patterned after that described in Krehbiel et al. (1996).

The architecture described above is also appropriate for a four-faced PPAR "weather only" WSR-88D replacement. The radar scan timeline would be apportioned between "standard" weather variable measurements—SHV observations of the six variables measured by the WSR-88D—and ice crystal alignment observations using a dual-channel CP basis and processing as outlined in Fig. 8.

Considering the antenna configuration in Fig. 7, we discuss the radar scan timeline using as an example, the 14-elevation-tilt (from 0.5° to 19.5°) WSR-88D VCP number 212. The WSR-88D requires 270 s to complete this VCP, although use of supplemental adaptive intravolume low-level scans (SAILS) or midvolume rescan of low-level elevations (MRLE) can provide more frequent updates of low-elevation angle tilts. By using three simultaneous receive beams, a four-faced PPAR could complete the VCP in 23 s. If the standard weather variables are updated once per minute, 63% of the radar timeline would therefore be available for ice crystal alignment observations. If the same set of elevation tilts were used, 1260 beam pointing angles would need to be surveilled in 3.1 s (0.63 × 5 s). Our notional CPI of 0.020 s would require that eight simultaneous receive beams be used for this function. In summary, the radar timeline would be divided into 5-s intervals with 1.9 s allocated to measurement of the standard weather variables and 3.1 s allocated to ice crystal alignment monitoring.

Use of multiple receive beams to increase the scan rate incurs a penalty in sensitivity, as the spoiled transmit beam's gain is reduced in proportion to the number of receive beams it must support. Because the PPAR average radiated power is likely to be an order-of-magnitude greater than that of the WSR-88D (appendix A of Weber et al. 2021), the 5-dB loss resulting from using three simultaneous beams for standard weather variable measurements would not reduce the PPAR's sensitivity below that of the WSR-88D. Similarly, the 9-dB loss for the larger beam cluster used for ice crystal monitoring would not affect the ability to meet our notional sensitivity for this function. Higher effective two-way sidelobes within the beam clusters are also of concern due to the flat response of the spoiled transmit beam. For the antenna in Fig. 7, sidelobes in the angles covered by adjacent simultaneous receive beams would be approximately −45 dB (Schvartzman

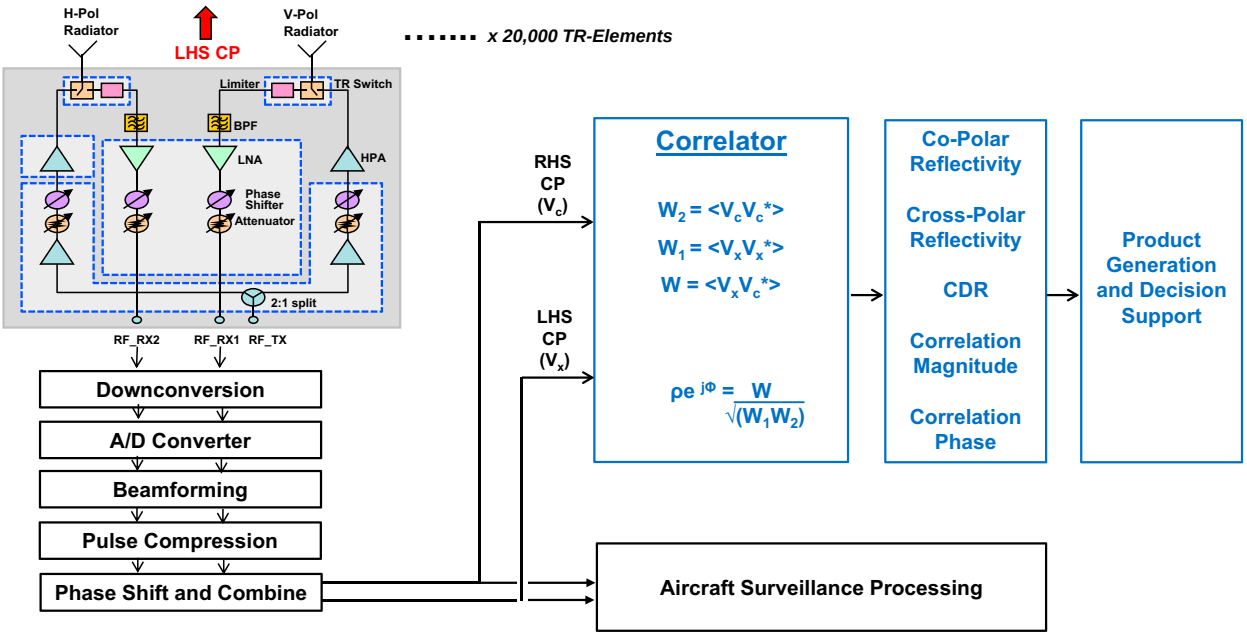

FIG. 8. Notional signal-processing flow for MPAR aircraft surveillance and ice crystal alignment monitoring functions.

et al. 2021) and might smear measured returns in regions of strong azimuthal gradients. Weber et al. (2017) show this effect can be mitigated for the standard weather variables using a data-adaptive method to vary the size of the beam clusters.

d. Rotating single-face planar array

Beginning in 2018, NOAA's phased array radar research emphasis shifted to a single-mission replacement system for the WSR-88D. Because the radar timeline would no longer be shared between weather and aircraft surveillance missions, a single-faced rotating array is of interest. This is likely to be more cost-effective than a multifaced system if it can decrease the volume scan time for standard weather variables to 60 s.

This configuration is more challenging, however, for crystal alignment monitoring given the 12 min^{-1} goal for volumetric observations. Small-aperture research phased array radars such as described in the last section of this article can rotate mechanically at rates this high, but an 8-m-diameter PPAR replicating the WSR-88D's beamwidth would practically need to rotate much more slowly.

As a concrete example, Fig. 9 illustrates a "sector RHI" rotating array scanning pattern for the standard weather variables, where azimuth-limited sectors (e.g., 30°) are electronically scanned at all elevation tilts as the array rotates in azimuth. The full volume scan is completed during one 360° rotation of the antenna at a rate of 6.7° s^{-1}. By spoiling the transmit beam and receiving simultaneously in five separately steered receive beams the time to execute the WSR-88D volume coverage pattern, VCP-212, is reduced from 270 to 54 s.

A parallel processor could monitor crystal alignment utilizing additional, time-multiplexed CP transmissions to estimate the necessary polarimetric variables at a much higher update rate within the array's azimuth-limited (90°) field of view. To free up radar timeline for this function, we suggest that the size of the beam clusters to measure the standard weather variables could be increased from 5 to 7, and the antenna rotation rate decreased from 6.7° to 6.0° s^{-1}. With these changes, the antenna would rotate through 360° in azimuth in 60 s, 64% of the radar timeline (39 s during each 1-min volume scan) would be used to measure the standard weather variables, and 36% for crystal alignment observations (1.8 s during each 5-s volume scan). Our 0.020-s CPI implies that 14 simultaneous receive beams would be needed for the crystal alignment observations. These changes to the beam cluster size used for measurement of standard weather variables throughout the VCP might degrade their quality, as the use of larger beam clusters exacerbates the azimuthal smearing challenge discussed above and reduces the SNR by 1.5 dB. Operational users might choose not to accept reduced data quality when there are threats such as tornadoes, large hail, or severe winds, but in other circumstances the tradeoffs might be worthwhile.

The rotating antenna configuration would unavoidably produce significant temporal gaps in the 5-s-update crystal alignment observations. In the example above, at any azimuth angle three successive crystal observations would be followed by nine "missed" observations while the azimuth angle is not in the antenna's field of view. We conjecture that the important scientific and operational information provided by the crystal alignment observations would be captured during the 15-s observation period, and that changes in the standard weather variables, large-scale electric field structure, or large-scale microphysical characteristics of the storm would be small during the 45 s when observations are missing at a given azimuth angle. This conjecture, of course, needs to be validated experimentally as will be discussed in the last section.

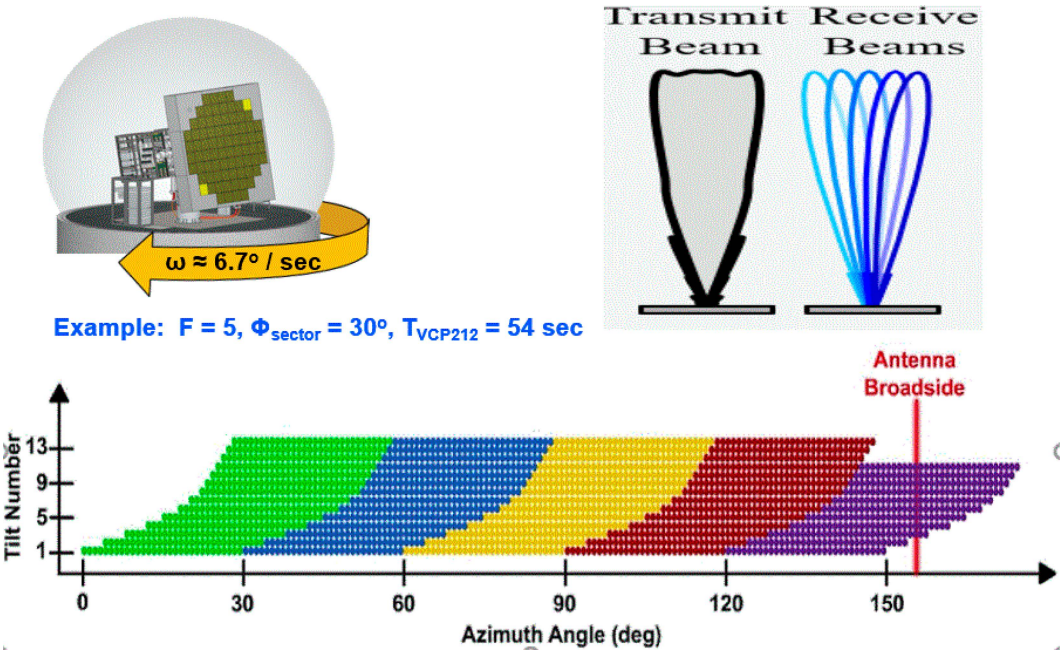

FIG. 9. Sector RHI scanning pattern for a rotating, single-faced phased array radar. The antenna rotation rate is synchronized to the time required to complete each azimuth-limited sector scan of all elevation tilts. A spoiled transmit beam and cluster of five digitally formed receive beams increases the scan rate by 5 without change to the CPI for each radial [this figure is adapted from Schvartzman et al. (2021)].

We conclude that in terms of radar timeline, either a four-faced stationary or single-faced rotating phased array could support the ice crystal monitoring function for nonsevere thunderstorms, in parallel with observations of the standard weather variables. Some compromises in these latter observations would be required to free up radar timeline, in particular, use of larger beam clusters that reduce sensitivity and increase the possibility of spatial smearing as discussed. Determining whether such trades are warranted will require in-depth evaluation of the possible operational benefits of the crystal alignment observations.

Given the importance of severe storm applications, additional research is needed to develop and validate adaptive scanning methods that could enable a PPAR to provide temporally resolved crystal alignment observations in severe storms with very high flash rates. By limiting scanning to azimuth/elevation angles where useful observations are likely to be obtained the update rate could be significantly increased. For example, the "persistent" alignment volume observed in the 29 April 2016 case study extended in altitude over only approximately 1/4 of the depth of the storm at the azimuth angle we sampled. Alternately, one could use storm centroids or other features to identify volumes where high flash rates are likely and target scanning to such volumes to improve the temporal sampling of depolarization streaks without adding significant overall scan time.

A significant technical challenge arises from the cross-polarized fields that occur when PPARs are electronically steered away from the principal horizontal or vertical planes (Zhang et al. 2011). Both architectures discussed assume that the beam will be steered over 90° in azimuth and to elevation angles well above the principal horizontal plane. Techniques for mitigating this inherent depolarization (Fulton et al. 2018) so that signal changes due to crystal alignment can be characterized are an important aspect of the research recommended in our last section.

4. Discussion

NSSL and its research and development partners have developed two PPAR demonstrators that are well suited to address research questions raised by the crystal alignment observation concept described in this article. The Advanced Technology Demonstrator (ATD), developed by NSSL, Massachusetts Institute of Technology Lincoln Laboratory, the University of Oklahoma (OU), and General Dynamics, is a 4-m-diameter S-band PPAR (Hondl and Weber 2019; Weber et al. 2021) that utilizes an overlapped subarray architecture as described in section 3. It can operate in SHV, CP, or AHV polarization bases. The broadside beamwidth is 1.5° and up to 10 simultaneous digital receive beams can be formed. Experiments could be conducted with the radar timeline dedicated to crystal alignment observations in which case a 90° by 30° sector (1380 beam positions) could be scanned every 2.8 s with a CPI of 0.020 s. Alternately, the pattern described above in which standard weather variable measurements and crystal alignment observations share the radar timeline, could be demonstrated.

The University of Oklahoma Advanced Radar Research Center (ARRC) has developed a truck-mounted, C-band Polarimetric Atmospheric Imaging Radar (PAIR) (Salazar et al. 2019).

PAIR transmits with a spoiled 20° elevation beam and digitally forms receive beams to generate a cluster of 1.5° pencil beams spanning the elevation extent of the transmit beam. The antenna scans 360° in azimuth in approximately 6 s. The volume scan update rate (10 min^{-1}), CPI (0.025 s) and sensitivity (18 dBZ at 100 km) provide high-quality aligned crystal observations. Because electronic scanning is only in the principal elevation plane, cross-polarized fields due to the array element patterns will be minimal.

Particularly if operated in a coordinated measurement campaign where the parent storm is well characterized, these two radars could provide unprecedented volumetric observations of the distribution, parameters, and temporal variation of aligned crystals in thunderclouds. As a concrete, experimental plan we recommend that multiple mobile and fixed radars be deployed in central Oklahoma to allow for high-temporal-resolution storm observations and multiple Doppler wind retrievals over a significant domain. Available polarimetric radar assets include the operational WSR-88D (KTLX) southeast of Oklahoma City, the NSSL experimental WSR-88D (KOUN) in Norman, and truck- or trailer-mounted deployable C- and X-band radars operated by NSSL and OU. The OLMA can provide continuous, high-resolution imaging of lightning activity characterizing its temporal rate and spatial structure. Electric field meters deployed at Oklahoma Mesonetwork sites in central Oklahoma could provide valuable measurements characterizing the large-scale electrical structure of the observed storms.

Ivić et al. (2022) describe additional X- and C-band PPAR demonstrators developed by researchers in the United States, Japan, and China that could also be used to explore the capabilities and applications of PPAR for ice crystal alignment monitoring. For example, since 2018 researchers at the Tokyo Metropolitan University and Toshiba have operated an X-band PPAR in the Tokyo metropolitan area. This planar array transmits using four to seven fan beams spanning angles up to 90° in the principal elevation plane and digitally synthesizes 1° receive beams. The array rotates mechanically in azimuth and normally completes a volume scan in approximately 60 s. In research mode, the volume scan time can be reduced to approximately 10 s. Like the OU PAIR, this PPAR operates fundamentally in a rapid-update RHI mode and could be configured to provide valuable ice crystal alignment observations for storms in Japan.

Observations such as those described above could be used to address important research questions such as the following:

(i) Can crystal alignment monitoring reliably discriminate stratiform and nonprecipitating anvil cloud regions surrounding active thunderclouds that are likely to produce cloud-to-ground lightning from those that are not? This could be important in improving public safety and decision support for ground operations that are sensitive to lightning.

(ii) Can crystal alignment monitoring be used to assess the likelihood of triggered lightning in clouds that are not producing natural lightning? This capability would be extremely valuable for the rapidly expanding commercial space industry, where triggered lightning during launch operations is a major safety concern.

(iii) Are there consistent signatures in the crystal alignment data that could help forecasters diagnose severe weather conditions? Can these be integrated with established polarimetric signatures to improve warning skill? Researcher A. V. Ryzhkov (2016, personal communication), for example, suggested that direct observation of aligned ice crystal volumes above Z_{DR} columns could better define the intensity and vertical extent of storm updrafts.

(iv) What are appropriate DA techniques for incorporating crystal alignment observations into numerical models and how much benefit do they provide in improving model analyses and forecasts?

(v) How can the crystal alignment observations be effectively integrated with other measurements of cloud electrification, in particular data from ground-based lightning detection networks and the NOAA Geostationary Environmental Satellite GLM sensor?

(vi) Can adaptive scanning methods mitigate challenges in resolving the temporal variation of crystal alignment structures in severe thunderstorms where flash rates may significantly exceed realistic PPAR volume scanning rates? Do the operational benefits of the crystal alignment observations in such storms add significantly to those achievable with ground- or space-based lightning detection systems?

(vii) Can the impact of cross-polarized fields resulting from PPAR beam steering be effectively mitigated through compensation based on array calibration and/or digital processing such as the phase coding method described by Ivić and Doviak (2016)?

As noted, NOAA is investing significant effort toward research and risk reduction for the PPAR alternative for a successor to the WSR-88D. The proposed research could help NOAA to assess the operational benefits of a PPAR ice crystal alignment monitoring capability and define necessary technical capabilities.

Acknowledgments. We are grateful for the support of the NOAA Office of Oceanic and Atmospheric Research (OAR) under Contract NA16OAR4320072 (author Zhang). Comments and suggestions from three anonymous reviewers have significantly improved the article.

Data availability statement. KTLX data are available from the National Centers for Environmental Information (https://www.ncei.noaa.gov/), and Earth Networks lightning data can be requested from the company (https://www.earthnetworks.com/product/lightning-data/).

REFERENCES

Bruning, E. C., and D. R. MacGorman, 2013: Theory and observations of controls on lightning flash size spectra. *J. Atmos. Sci.*, **70**, 4012–4029, https://doi.org/10.1175/JAS-D-12-0289.1.

Byrne, G. J., A. A. Few, and M. E. Weber, 1983: Altitude, thickness and charge concentration of charged regions of four

thunderstorms during TRIP 1981 based upon in situ balloon electric field measurements. *Geophys. Res. Lett.*, **10**, 39–42, https://doi.org/10.1029/GL010i001p00039.

Caylor, I. J., and V. Chandrasekar, 1996: Time-varying ice crystal orientation in thunderstorms observed with multiparameter radar. *IEEE Trans. Geosci. Remote Sens.*, **34**, 847–858, https://doi.org/10.1109/36.508402.

Deierling, W., W. A. Petersen, J. Latham, S. Ellis, and H. J. Christian, 2008: The relationship between lightning activity and ice fluxes in thunderstorms. *J. Geophys. Res.*, **113**, D15210, https://doi.org/10.1029/2007JD009700.

Emersic, C., P. L. Heinselman, D. R. MacGorman, and E. C. Bruning, 2011: Lightning activity in a hail-producing storm observed with phased-array radar. *Mon. Wea. Rev.*, **139**, 1809–1825, https://doi.org/10.1175/2010MWR3574.1.

Fierro, A. O., Y. Wang, J. Gao, and E. R. Mansell, 2019: Variational assimilation of radar data and GLM lightning-derived water vapor for the short-term forecasts of high-impact convective events. *Mon. Wea. Rev.*, **147**, 4045–4069, https://doi.org/10.1175/MWR-D-18-0421.1.

Fulton, C., J. Salazar, D. Zrnic, D. Mirkovic, I. Ivić, and D. Doviak, 2018: Polarimetric phased array calibration for large-scale multi-mission radar applications. *2018 IEEE Radar Conf. (RadarConf18)*, Oklahoma City, OK, Institute of Electrical and Electronics Engineers, 1272–1277, https://doi.org/10.1109/RADAR.2018.8378746.

Gatlin, P. N., and S. J. Goodman, 2010: A total lightning trending algorithm to identify severe thunderstorms. *J. Atmos. Oceanic Technol.*, **27**, 3–22, https://doi.org/10.1175/2009JTECHA1286.1.

Heitkemper, L., R. F. Price, and D. B. Johnson, 2008: Lightning-warning systems for use by airports. ACRP Rep. 8, 81 pp., https://www.idc-online.com/technical_references/pdfs/electrical_engineering/acrp_rpt_008.pdf.

Hendry, A., and G. C. McCormick, 1976: Radar observations of the alignment of precipitation particles by electrostatic fields in thunderstorms. *J. Geophys. Res.*, **81**, 5353–5357, https://doi.org/10.1029/JC081i030p05353.

——, and Y. M. M. Antar, 1982: Radar observations of polarization characteristics and lightning-induced realignment of atmospheric ice crystals. *Radio Sci.*, **17**, 1243–1250, https://doi.org/10.1029/RS017i005p01243.

Hondl, K., and M. Weber, 2019: NOAA's meteorological phased array radar research program. *2019 IEEE Int. Symp. on Phased Array System and Technology (PAST)*, Waltham, MA, Institute of Electrical and Electronics Engineers, 1–6, https://doi.org/10.1109/PAST43306.2019.9020994.

Hubbert, J. C., S. M. Ellis, W.-Y. Chang, and Y.-C. Liou, 2014a: X-band polarimetric observations of cross coupling in the ice phase of convective storms in Taiwan. *J. Appl. Meteor. Climatol.*, **53**, 1678–1695, https://doi.org/10.1175/JAMC-D-13-0360.1.

——, ——, ——, S. Rutledge, and M. Dixon, 2014b: Modeling and interpretation of S-band ice crystal depolarization signatures from data obtained by simultaneously transmitting horizontally and vertically polarized fields. *J. Appl. Meteor. Climatol.*, **53**, 1659–1677, https://doi.org/10.1175/JAMC-D-13-0158.1.

——, W. Deierling, P. Kennedy, and M. Dixon, 2015: Detection of electrification with the co-to-cross correlation coefficient with storm microphysics analysis. *37th Conf. on Radar Meteorology*, Norman, OK, Amer. Meteor. Soc., 63, https://ams.confex.com/ams/37RADAR/webprogram/37RADAR.html.

——, J. W. Wilson, T. M. Weckwerth, S. M. Ellis, M. Dixon, and E. Loew, 2018: S-Pol's polarimetric data reveal detailed storm features (and insect behavior). *Bull. Amer. Meteor. Soc.*, **99**, 2045–2060, https://doi.org/10.1175/BAMS-D-17-0317.1.

Ivić, I. R., and R. J. Doviak, 2016: Evaluation of phase coding to mitigate differential reflectivity bias in polarimetric PAR. *IEEE Trans. Geosci. Remote Sens.*, **54**, 431–451, https://doi.org/10.1109/TGRS.2015.2459047.

——, M. D. Conway, S. M. Torres, J. S. Herd, D. S. Zrnic, and M. E. Weber, 2022: Meteorological polarimetric phased array radar. *Polarimetric Radar Signal Processing*, A. Aubry, A. De Maio, and A. Farina, Eds., Institute of Engineering and Technology, 433–479.

Jones, T. A., K. Knopfmeier, D. Wheatley, G. Creager, P. Minnis, and R. Palikondo, 2016: Storm-scale data assimilation and ensemble forecasting with the NSSL experimental warn-on-forecast system. Part II: Combined radar and satellite data experiments. *Wea. Forecasting*, **31**, 297–327, https://doi.org/10.1175/WAF-D-15-0107.1.

Krehbiel, P., T. Chen, S. McCray, W. Wilson, G. Gray, and M. Brook, 1996: The use of dual channel circular polarized radar observations for remotely sensing storm electrification. *Meteor. Atmos. Phys.*, **59**, 65–82, https://doi.org/10.1007/BF01032001.

MacGorman, D. R., 1993: Lightning in tornadic storms: A review. *The Tornado: Its Structure, Dynamics, Prediction, and Hazards*, *Geophys. Monogr.*, Vol. 79, Amer. Geophys. Union, 173–182, https://doi.org/10.1029/GM079p0173.

Marshall, T. C., and W. P. Winn, 1982: Measurements of charged precipitation in a New Mexico thunderstorm: Lower positive charge centers. *J. Geophys. Res.*, **87**, 7141–7157, https://doi.org/10.1029/JC087iC09p07141.

Mazzetti, T. O., and H. E. Fuelberg, 2017: An analysis of total lightning flash rates over Florida. *J. Geophys. Res. Atmos.*, **122**, 12 812–12 826, https://doi.org/10.1002/2017JD027579.

McCormick, G. C., and A. Hendry, 1979: Radar measurement of precipitation-related depolarization in thunderstorms. *IEEE Trans. Geosci. Electron.*, **17**, 142–150, https://doi.org/10.1109/TGE.1979.294641.

Melnikov, V., D. S. Zrnić, M. E. Weber, A. O. Fierro, and D. R. MacGorman, 2019: Electrified cloud areas observed in the SHV and LDR radar modes. *J. Atmos. Oceanic Technol.*, **36**, 151–159, https://doi.org/10.1175/JTECH-D-18-0022.1.

Metcalf, J. I., 1995: Radar observations of changing orientations of hydrometeors in thunderstorms. *J. Appl. Meteor.*, **34**, 757–772, https://doi.org/10.1175/1520-0450(1995)034<0757:ROOCOO>2.0.CO;2.

——, 1997: Temporal and spatial variations of hydrometeor orientations in thunderstorms. *J. Appl. Meteor.*, **36**, 315–321, https://doi.org/10.1175/1520-0450(1997)036<0315:TASVOH>2.0.CO;2.

NWS, 2015: NOAA/National Weather Service radar functional requirements. NOAA Tech. Doc., 58 pp., www.roc.noaa.gov/WSR88D/PublicDocs/NOAA_Radar_Functional_Requirements_Final_Sept%202015.pdf.

Rutledge, S. A., E. R. Williams, and W. A. Petersen, 1993: Lightning and electrical structure of mesoscale convective systems. *Atmos. Res.*, **29**, 27–53, https://doi.org/10.1016/0169-8095(93)90036-N.

Ryzhkov, A. V., and D. S. Zrnić, 2007: Depolarization in ice crystals and its effect on radar polarimetric measurements. *J. Atmos. Oceanic Technol.*, **24**, 1256–1267, https://doi.org/10.1175/JTECH2034.1.

Salazar, J. L., and Coauthors, 2019: An ultra-fast scan C-band Polarimetric Atmospheric Imaging Radar (PAIR). *2019 IEEE Int. Symp. on Phased Array System & Technology (PAST)*,

Waltham, MA, Institute of Electrical and Electronics Engineers, 1–5, https://doi.org/10.1109/PAST43306.2019.9021042.

Schenkman, A. D., M. Xue, A. Shapiro, K. Brewster, and J. Gao, 2011: The analysis and prediction of the 8–9 May 2007 Oklahoma tornadic mesoscale convective system by assimilating WSR-88D and CASA radar data using 3DVAR. *Mon. Wea. Rev.*, **139**, 224–246, https://doi.org/10.1175/2010MWR3336.1.

Schultz, C. J., W. A. Petersen, and L. D. Carey, 2009: Preliminary development and evaluation of lightning jump algorithms for the real-time detection of severe weather. *J. Appl. Meteor. Climatol.*, **48**, 2543–2563, https://doi.org/10.1175/2009JAMC2237.1.

——, ——, and ——, 2011: Lightning and severe weather: A comparison between total and cloud-to-ground lightning trends. *Wea. Forecasting*, **26**, 744–755, https://doi.org/10.1175/WAF-D-10-05026.1.

——, L. D. Carey, E. V. Schultz, and R. L. Blakeslee, 2015: Insight into the kinematic and microphysical processes that control lightning jumps. *Wea. Forecasting*, **30**, 1591–1621, https://doi.org/10.1175/WAF-D-14-00147.1.

Schvartzman, D., M. Weber, S. Torres, H. Thomas, D. Zrnić, and I. Ivić, 2021: Scanning concepts and architectures supporting rotating meteorological phased-array radar. *37th Conf. Environmental. Information Processing*, Online, Amer. Meteor. Soc., 10.8, https://ams.confex.com/ams/101ANNUAL/meetingapp.cgi/Paper/379726.

Stailey, J. E., and K. D. Hondl, 2016: Multifunction phased array radar for aircraft and weather surveillance. *Proc. IEEE*, **104**, 649–659, https://doi.org/10.1109/JPROC.2015.2491179.

Steiner, M., W. Deierling, K. Ikeda, and R. G. Bass, 2014: Ground delays from lightning ramp closures and decision uncertainties. *Air Traffic Control Quart.*, **22**, 223–249, https://doi.org/10.2514/atcq.22.3.223.

Stensrud, D. J., and J. Gao, 2010: Importance of horizontally inhomogeneous environmental initial conditions to ensemble storm-scale radar data assimilation and very short-range forecasts. *Mon. Wea. Rev.*, **138**, 1250–1272, https://doi.org/10.1175/2009MWR3027.1.

Weber, M. E., and M. L. Stone, 1995: Low altitude wind shear detection using airport surveillance radars. *IEEE Aerosp. Electron. Syst.*, **10**, 3–9, https://doi.org/10.1109/62.387970.

——, H. J. Christian, A. A. Few, and M. F. Stewart, 1982: A thundercloud electric field sounding: Charge distribution and lightning. *J. Geophys. Res.*, **87**, 7158–7169, https://doi.org/10.1029/JC087iC09p07158.

——, J. Y. N. Cho, J. S. Herd, J. M. Flavin, W. E. Benner, and G. S. Torok, 2007: The next-generation multimission U.S. surveillance radar network. *Bull. Amer. Meteor. Soc.*, **88**, 1739–1752, https://doi.org/10.1175/BAMS-88-11-1739.

——, ——, and H. G. Thomas, 2017: Command and control for multifunction phased array radar. *IEEE Trans. Geosci. Remote Sens.*, **55**, 5899–5912, https://doi.org/10.1109/TGRS.2017.2716935.

——, and Coauthors, 2021: Towards the next generation operational meteorological radar. *Bull. Amer. Meteor. Soc.*, **102**, E1357–E1383, https://doi.org/10.1175/BAMS-D-20-0067.1.

Weinheimer, A. J., and A. A. Few, 1987: The electric field alignment of ice particles in thunderstorms. *J. Geophys. Res.*, **92**, 14 833–14 844, https://doi.org/10.1029/JD092iD12p14833.

Williams, E. R., M. E. Weber, and R. E. Orville, 1989: The relationship between lightning type and convective state of thunderclouds. *J. Geophys. Res.*, **94**, 13 213–13 220, https://doi.org/10.1029/JD094iD11p13213.

——, and Coauthors, 1999: The behavior of total lightning activity in severe Florida thunderstorms. *Atmos. Res.*, **51**, 245–265, https://doi.org/10.1016/S0169-8095(99)00011-3.

Winn, W. P., G. W. Schwede, and C. B. Moore, 1974: Measurements of electric fields in thunderclouds. *J. Geophys. Res.*, **79**, 1761–1767, https://doi.org/10.1029/JC079i012p01761.

——, C. B. Moore, and C. R. Holmes, 1981: Electric field structure in an active part of a small, isolated thundercloud. *J. Geophys. Res.*, **86**, 1187–1193 https://doi.org/10.1029/JC086iC02p01187.

Yoshida, S., T. Adachi, K. Kusunoki, S. Hayashi, T. Wu, T. Ushio, and E. Yoshikawa, 2017: Relationship between thunderstorm electrification and storm kinetics revealed by phased array weather radar. *J. Geophys. Res. Atmos.*, **122**, 3821–3836, https://doi.org/10.1002/2016JD025947.

Yussouf, N., J. S. Kain, and A. J. Clark, 2016: Short-term probabilistic forecasts of the 31 May 2013 Oklahoma tornado and flash flood event using a continuous-update-cycle storm-scale ensemble system. *Wea. Forecasting*, **31**, 957–983, https://doi.org/10.1175/WAF-D-15-0160.1.

Zhang, G., R. J. Doviak, D. S. Zrnić, R. Palmer, L. Lei, and Y. Al-Rashid, 2011: Polarimetric phased-array radar for weather measurement: A planar or cylindrical configuration? *J. Atmos. Oceanic Technol.*, **28**, 63–73, https://doi.org/10.1175/2010JTECHA1470.1.

Zrnic, D. S., and Coauthors, 2007: Agile beam phased array radar for weather observations. *Bull. Amer. Meteor. Soc.*, **88**, 1753–1766, https://doi.org/10.1175/BAMS-88-11-1753.